

# Dynamic Mobile Robots for Emergency Surveillance and Situational Awareness

Laura Ray<sup>1</sup>, James Joslin<sup>1</sup>, John Murphy<sup>1</sup>, Jon Barlow<sup>1</sup>, Devin Brande<sup>1</sup>, and Devin Balkcom<sup>2</sup>

*Dartmouth College*

*8000 Cummings Hall, Hanover NH 03755*

*e-mail: lray@dartmouth.edu*

**Abstract— This paper investigates cooperative control for groups of high speed, low cost mobile robots. The control framework, comprised of a global, dynamic path planning and control method and local wheel slip controllers on each robot, is intended to promote ubiquitous and affordable “peek” robot control in situations where rapid response is vital. The influence of the control framework on group response in cooperative formation control under two different mobility conditions is demonstrated by simulation. In order to evaluate the control framework, a low-cost 10-kg robot is designed for speed and acceleration of up to 10 m/s and 4 m/s<sup>2</sup>, respectively. A dynamic model of the robot is developed, with attention to representation of tire-terrain characteristics for high-speed lightweight mobile robots.**

## I. INTRODUCTION

Emergency response scenarios involving large-scale casualties, release of hazardous substances, or the need to augment human responders will require inexpensive robots that can be deployed rapidly and whose positions can be reconfigured rapidly, with minimal human intervention. For example, sensing of concentration gradients of a substance over a region, triage support, and general situational awareness can benefit from teams of high-speed robots that are readily controlled by one operator. Commercial robots for keeping humans out of harm’s way have proven to be an indispensable component of military campaigns [1,2]. However, the affordability of even one such robot is limited for local first responders, and maintenance/upkeep can be beyond the budgets of many emergency response organizations.

The need for inexpensive high-speed robots, as well as for techniques to control large numbers of them in large-scale emergency response scenarios, is well-recognized. Ref. [3] classifies emergency response robots, with the class of “peek” robots defined as being capable of providing “rapid audio visual situational awareness, rapid HAZMAT detection, and data logging for subsequent team work.” High speed, inexpensive robots, if available, could meet the needs of local response agencies, and can be used in teams for surveillance tasks associated with large scale events. Ref. [4] presents an algorithm to aid robot motion planning and exploration in

rescue situations. In [5], a protocol is developed that would allow robot networks to locate resources and services efficiently in a dynamic environment. This paper contributes both the design of a high-speed robot testbed that can be used to explore control issues, and an initial control framework that is suitable for distributed control and accounts for the dynamic behaviour of the robots in diverse terrain.

The robot design is based on off-the-shelf components and a plastic-molded chassis, in order to study dynamic cooperative control. Attention to part count, manufacturability, and design for assembly provides a robot with an estimated unit cost of under \$5000 in quantities of 7 to 10 that can be fabricated using in-house facilities. We develop a dynamic model for a two-wheel-drive (2WD) configuration of the robot. Control issues encountered when introducing a high-speed robot within an existing distributed control scheme are illustrated using a potential function approach originally developed for (slow moving) point-mass robots. Because such methods address the general problem of cooperative control and path planning well, it is useful to adapt these methods to dynamic robots in a manner that allows for robust operation under a range of terrains, operating conditions, speeds, and initial conditions. A local slip controller for each robot provides robust, high-speed operation during cooperative formation control.

Section 2 summarizes the current design status and mathematical model of the robot. Section 3 describes the control framework, and Section 4 demonstrates the performance of the cooperative control framework.

## II. ROBOT DESIGN AND MODEL

The prototype robot, shown in Figure 1, is a reconfigurable design that permits the robot to operate either by two independently driven wheels with a trailing caster or four independently driven wheels. Both designs use differential steering without a suspension. For simplicity, we designed a common two-wheel body on which either the caster or an additional two-wheel assembly can be mounted. The body has a simple boxlike design with a removable lid. Drivetrain, electronic component supports, and mounting surfaces are incorporated within a rugged plastic chassis. Reinforcing ribs minimize deformation and vibration of the body. Structural analysis of the chassis shows that it provides sufficient

<sup>1</sup> Thayer School of Engineering and affiliate, Institute for Security Technology Studies

<sup>2</sup> Dept. of Computer Science and affiliate, Institute for Security Technology Studies

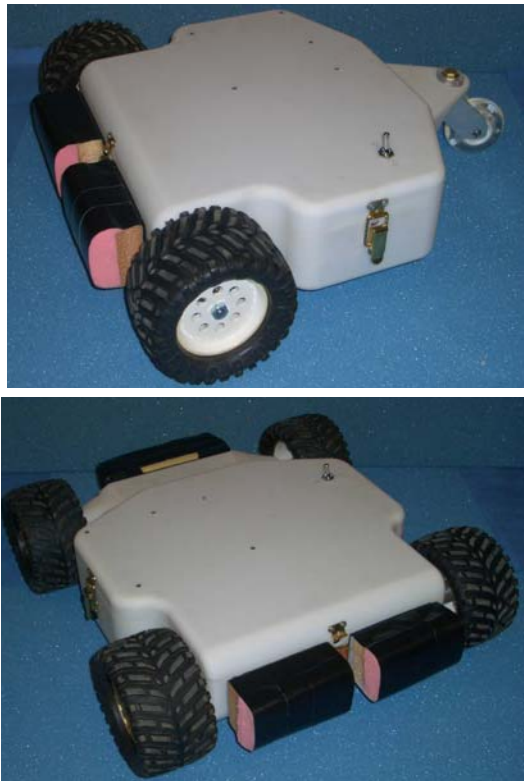


Figure 1 Robot prototype in two configurations -2WD, 4WD strength and rigidity for operation in terrain of moderate roughness, e.g., vegetation and rocky terrain. The ground clearance is 6-8 cm.

The number and complexity of fabricated parts is limited, with off-the-shelf components used when possible in order to simplify manufacturing, assembly, and maintenance. A 3 inch hard rubber rollerblade wheel serves as a caster with small surface area contact. The caster pivots on a commercial ball bearing to minimize resistance. To reconfigure from 2WD to 4WD, a two wheel unit mounts on a hollow bushing joint in the middle of the back end. This joint allows two wheels to pivot passively 60 degrees in either direction. With this articulated head the vehicle maintains ground contact with more wheels while driving over uneven terrain and is less likely to become high centered. A prototype chassis has been rapid-prototyped in ABS for design evaluation. Multiple copies of the chassis will be cast using a silicon mold and stronger polyurethane plastic.

The drivetrain is comprised of an EAD 24 volt brushless DC motor combined with a Neugart 3:1 planetary gearhead. This system delivers 0.27 N-m of torque to each wheel @ 1275 RPM with a peak efficiency of over 70%, providing 144 W of power for four motors and a targeted maximum speed of 10.1 m/s on hard surfaces. The motor-gearhead provides 1.5 N-m continuous stall torque at each driven wheel. Compact, inexpensive brushless motor controllers from Advanced Motion Controls use torque control to drive each motor. The wheels are standard scale model, non-inflatable, soft rubber tires with plastic hubs. Although the wheel size can be varied in the design, we use a 15.24 cm (6 in.) diameter 7.62 cm (3

in.) wide tire with rough tread in order to provide a large contact surface and increased traction. A simple inline drivetrain (Figure 2) independently drives each wheel. Each drivetrain requires three machined parts: a couple, an axle, and an outboard bearing housing. The bearing housing supports the axle with a commercial bearing from within the hub in order to minimize the required drivetrain space within the chassis. Two 24 volt NiMH batteries, each rated at 3.3 Ah provide over 1.5 hours of operation during start-stop operation.

The brain of the robot is a Z-World Jackrabbit 3100 microprocessor, programmed in Dynamic C. Sensors include GPS, angular rates and accelerations, wheel speed, and motor currents. The 2WD configuration allows for measurement of vehicle speed through the undriven caster to supplement GPS. Communication is implemented using a local wireless network. A combination of commercial and in-house developed electronics provides signal conditioning and input-output. Parts costs for a quantity of 7-10 robots are detailed in Table 1.

The prototype robot meets design specifications for a highly maneuverable robot platform to study dynamic cooperative control. The measured hard surface acceleration is 7 m/s<sup>2</sup>, yaw rate is one rev/sec, and measured maximum speed is 11 m/s, exceeding design expectations. The basic design could be augmented with an external payload fixed to the top of the vehicle, e.g., camera, laptop computer, and environmental sensors, providing a low cost, robust vehicle for SWAT teams and local enforcement agencies.

In order to study control and performance of dynamic mobile robots, an accurate vehicle dynamic model is required. Although many studies consider kinematics and dynamics of robot motion, few detailed models of tire-terrain interaction exist for lightweight robots. [6-8] consider slip between the wheel and terrain contact for modelling of a wheeled robot. [9] develops an empirical model for slip between a hard

TABLE I: PER ROBOT COST SUMMARY FOR LOTS OF 10 ROBOTS

Part	Cost
(4) Brushless DC motors, gearheads, and motor controllers	\$ 2525
Chassis (includes tooling)	\$ 100
Machined components, bearings, and wheels	\$ 130
Batteries	\$ 125
Microcontroller and wireless link	\$ 440
Sensors, electronics, power converters, wiring harness	\$ 1250
GPS receiver	\$ 200
Total:	\$4770 (4 wheel) \$3560(2 wheel)

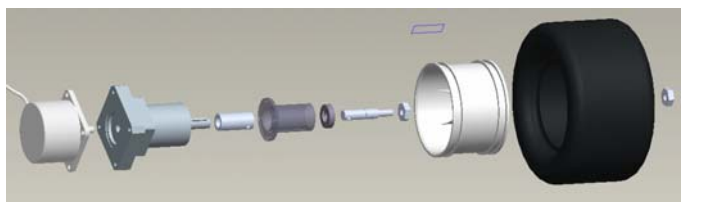


Figure 2 Drivetrain showing motor, gearhead, machined components, and wheel assembly

rubber roller wheel and ground for an omni-directional robot, and measures actual characteristics to characterize the sliding dynamics. The empirical model of sliding dynamics in [9] relates the friction coefficient to the sliding velocity components in the direction of wheel rotation and transverse direction through an arctangent function. This provides tire force saturation, but without the decay in force with slip or velocity commonly found in larger vehicles. Due to the specific construction of the wheel, the model does not generalize to soft rubber tires. [10] develops a platform for measuring the resistance of rigid tires on rigid and deformable terrain for planetary rovers and also finds an arctangent relationship between sliding velocity and force.

Sliding velocities are related to traditional definitions of wheel slip and slip angle. However, the vehicles used in the studies above are relatively slow, and therefore velocity dependence of the tire force models is not explicitly evaluated. Since detailed tire force models for high-speed, lightweight wheeled robots are not available at this time, we scale a traditional tire force model [11] to a small mobile robot with rubber tires. This model describes the friction or adhesion coefficient developed at the contact patch between the rubber tire and driving surface as a function of wheel slip and slip angle. An example of resulting tire forces for a 10 kg vehicle on both dry and wet hard surfaces, is shown in Figure 4. The maximum tire force and slip and slip angle at which the maximum occurs can be adjusted using model parameters. The restoring moment,  $M_z$  is assumed to be proportional to slip angle. Future experimental studies will measure actual tire force characteristics on a variety of surfaces – gravel, sand, carpet, asphalt, vegetated – in order to develop a body of knowledge for modeling lightweight, high speed mobile robots.

The dynamic model is developed here for the two-wheeled robot configuration. The forces from each driven wheel combine to exert a net force, which is modelled using a three degree-of-freedom rigid-body model. Including the two wheel degrees of freedom, the equations of motion in body-fixed axes are

$$\dot{v}_x = v_y r + \frac{1}{m}(F_{xl} + F_{xr} + F_{xres}) \quad (1)$$

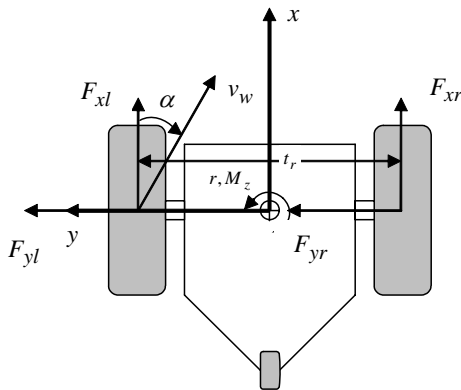


Figure 3 Definition of tire forces and slip angle.

$$\dot{v}_y = -v_x r + \frac{1}{m}(F_{yl} + F_{yr} + F_{yres}) \quad (2)$$

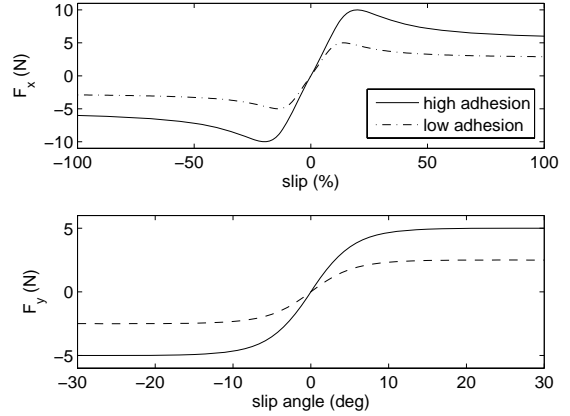


Figure 4 Longitudinal and lateral tire forces for a low adhesion and high adhesion surface

TABLE II: VEHICLE MODEL PARAMETERS

Description	Symbol	Value
Track width	$t_r$	0.3 m
Wheel radius	$R$	0.076 m
Vehicle mass	$m$	9 kg
Yaw moment of inertia	$I_{zz}$	0.203 kg-m <sup>2</sup>
Wheel moment of inertia	$I_w$	0.0007 kg-m <sup>2</sup>

$$\dot{r} = \frac{1}{I_{zz}} \left[ (F_{xr} - F_{xl}) \frac{t_r}{2} + M_z - M_{res} r \right] \quad (3)$$

$$\dot{\omega}_l = (T_l - F_{xl}R - b\omega_l) \frac{1}{I_w} \quad (4)$$

$$\dot{\omega}_r = (T_r - F_{xr}R - b\omega_r) \frac{1}{I_w} \quad (5)$$

where the  $v_x, v_y, r, \omega_l$ , and  $\omega_r$  are the longitudinal and lateral velocities of the vehicle center-of-mass, yaw rate about the  $z$ -axis through the center-of-mass, and wheel angular velocities about their axes of rotation; and  $F_{xl}, F_{xr}, F_{yl}$ , and  $F_{yr}$  are the tire forces along body-fixed Cartesian coordinate axes, as defined in Figure 3.  $M_z$  is the net restoring moment provided by both tires. Resistance terms  $F_{xres}, F_{yres}$ ,  $b\omega_l$ ,  $b\omega_r$  and  $M_{res}$  represent the natural mobility and drivetrain mechanical resistance. These forces and moments contain fixed Coulomb-static friction and/or a velocity-dependent (viscous) damping term. Other constants are defined in Table 2. The center-of-mass is assumed to be along the axis of the wheels, as shown in Figure 3.

### III. CONTROL METHOD

The artificial potential function approach provides path planning and navigation along a path [12]-[14]. Given a suitable potential function  $V$ , the control law takes the form

$$T(r, \dot{r}) = -\nabla V(r) + d(r, \dot{r}) \quad (6)$$

where  $r$  and  $\dot{r}$  are the generalized position and velocity of the robot,  $d(r, \dot{r})$  is a dissipative function, and  $T(r, \dot{r})$  is a control

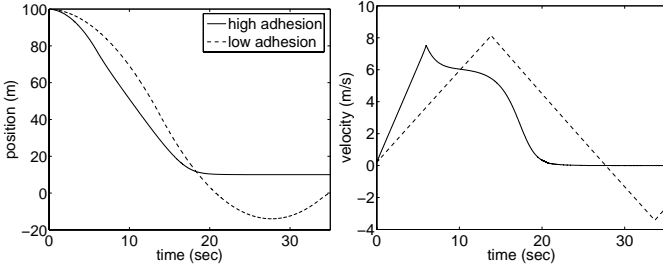


Figure 5 Distance from virtual leader and speed vs. time for a single robot, slip setpoint control inactive.

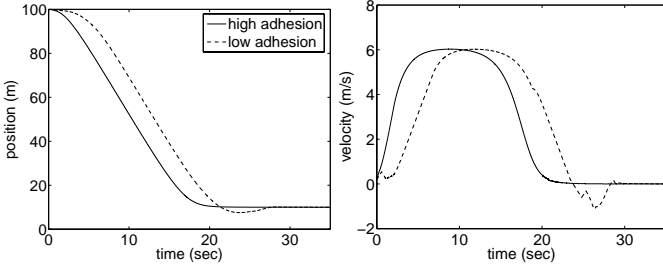


Figure 6 Distance from virtual leader and speed vs. time for a single robot, slip setpoint control active.

input [14]. The instantiation of this method using a radial potential function described in [15] is used here, providing dynamic path planning and global control as the robots move with respect to each other. The field contains both physical vehicles and virtual leaders. In the context of an emergency response scenario, the virtual leader could be a human operator that moves in the field with the robots, a point in space, teleoperated by a human operator, or a real robot teleoperated by a human. Each entity has a potential function defined by

$$V = V_h + V_d \quad (7)$$

where

$$V_d = \begin{cases} \alpha_d \left( \ln(r_{ij}) + \frac{d_o}{r_{ij}} \right) & 0 < r_{ij} < d_1 \\ \alpha_d \left( \ln(d_1) + \frac{d_o}{d_1} \right) & r_{ij} \geq d_1 \end{cases} \quad (8)$$

is the inter-vehicle potential and

$$V_h = \begin{cases} \alpha_h \left( \ln(h_{ik}) + \frac{h_o}{h_{ik}} \right) & 0 < h_{ik} < h_1 \\ \alpha_h \left( \ln(h_1) + \frac{h_o}{h_1} \right) & h_{ik} \geq h_1 \end{cases} \quad (9)$$

is the potential associated with a real or virtual leader.  $r_{ij}$  and  $h_{ik}$  are distances between robot  $i$  and  $j$  and robot  $i$  and leader  $k$ , respectively.  $d_o$ ,  $h_o$ ,  $d_1$ , and  $h_1$  are scalar parameters governing the domain of repulsion and attraction between robots and leaders.  $d_o$  and  $h_o$  are the distances around a robot and leader, respectively, at which the potential “well” is at its minimum.  $\alpha_d$ ,  $\alpha_h$  are scalar control gains governing

the “depth” or magnitude of a well around individual robots or leaders, i.e., minima of the potential functions associated with individual robots and leaders, respectively. A nonlinear

dissipative function  $\sum_k f_{dis} \frac{v_i^n}{h_{ik}^m}$  acts opposite to the

direction of the velocity vector, where  $v_i$  is the speed of robot  $i$ , and  $f_{dis}$  is a scalar gain. This functional form promotes robust overdamped responses during formation control, improving robustness for varied terrain characteristics.

The result of eq. 6 with potential function defined by eq. 7-9 is a commanded force vector for each robot, along the gradient of the potential field, comprised of distance-dependent contributions from each robot and leader, and a dissipative term opposite the robot’s velocity vector. The leader potential shepherds the vehicles either to flock to within a distance  $h_o$  of the leader while maintaining an inter-vehicle distance  $d_o$ , or to follow a moving virtual leader at a distance  $h_o$ , while maintaining inter-vehicle distances. Alternate formations can be accommodated by changing the form of the potential function and/or parameters for individual vehicles. Obstacles found by any robot or known *a priori* can be accommodated by including an obstacle potential term.

Potential function approaches were originally developed for point mass robots. The maximum velocity achieved along a trajectory for point masses depends heavily on the scalar control gains  $\alpha_d$  and  $\alpha_h$ . For simple particle dynamics, it is straightforward to choose these gains and a corresponding linear (viscous) dissipative force that targets a certain peak velocity and provides an overdamped response; given sufficient actuator bandwidth and power, arbitrary bandwidth is achieved for a point mass, along with overdamped trajectory following. When a similar control method is applied to a dynamic vehicle, as the control bandwidth increases demanding higher vehicle velocities and accelerations, tires saturate causing loss of traction. For a wheeled robot on an arbitrary surface, a change in surface adhesion has the same effect as increasing the potential function scalar gains and thus would require modification of the dissipative term to avoid oscillatory or unstable behavior. This relationship between the dynamics and dissipation requires an additional control component, e.g., sensing and accommodating adhesion conditions for each individual robot.

Here, we demonstrate behaviors exhibited for a robot with a fixed potential function and varying surface adhesion. Fig. 5 shows two time histories of distance from virtual leader for a single robot (i.e.,  $\alpha_h > 0$  and  $\alpha_d = 0$ ), with dynamics governed by eq. 3-7 and tire force characteristics shown in Fig. 4. Potential function parameters are set such that the maximum force command from eq. 6 is matched to the maximum tractive force on the high adhesion surface. The robot is pointed directly towards a virtual leader at  $t=0$  (i.e., no steering). With high adhesion and a sufficiently large dissipative force coefficient  $f_{dis}$ , well-damped motion results

and the robot achieves a peak velocity of 8 m/s (solid line). Holding the scalar control gains constant, a loss in adhesion results in poorly damped motion (dashed line), which, if active in a field of multiple robots, could induce poor group dynamics.

Increasing the dissipative force could recover the well-damped behavior on the low adhesion surface; however, mapping the dissipative force parameters to surface condition would be difficult and costly to establish and would effectively provide only open-loop adaptation to surface condition. Instead, a local slip-based traction controller is designed to maintain stability and robust performance on varying terrain. The local slip controller assumes the availability of a slip estimation scheme as reported in [16], which requires a sensor set comprised of wheel speeds,  $x$ - and  $y$ - accelerations, yaw rate, and vehicle speed. The slip estimation method is currently under evaluation for the differentially-steered mobile robot.

Slip control mode is triggered when the potential function commands a force that exceeds the maximum traction capability of the robot. Slip is then controlled at a setpoint just below the peak of the tire force curves using a PID controller. Figure 6 shows the motion of a single robot on high and low adhesion surfaces, with the same potential function and dissipative force parameters as in Fig. 5, and slip control active. On the high adhesion surface, slip control is triggered only briefly during the trajectory, as the potential function parameters are set to avoid force commands that saturate the tires. While the maximum velocity along the trajectory is lower than in Fig. 5, only a modest increase in time to reach the target is noted. On the low adhesion surface, local slip control increases damping significantly, allowing the vehicle to perform the maneuver in under 40 seconds, compared with under 25 seconds on the high adhesion surface.

Eq. 6 provides a vector force (magnitude and direction) to be applied to each robot. A steering control law must preserve the vector force to follow the intended path. A steering control law is introduced such that the total torque on two wheels is directly proportional to the force magnitude up to the adhesion limit, while the error between the vehicle heading and force direction (e.g., the bearing error) proportions the total torque between the two wheels. There are many ways to proportion the torque in a differentially steered vehicle. One could turn the vehicle around a vertical axis through its center-of-mass until the vehicle is pointed in the correct direction, and then proceed forward, or one could turn with a finite radius. In order to generalize this study to Ackerman-steered robots, we use a proportioning scheme based on bearing error. The magnitude of the total applied torque,  $T$ , is from eq. 6, and the torques on each wheel are

$$T_l = (1 - p)T \quad (10)$$

$$T_r = (1 + p)T \quad (11)$$

$p$  is a proportioning parameter normalized to  $\pm 1$  and derived using a PID control law based on bearing error,  $\phi_d - \phi$ , where

$\phi_d$  is the direction of the force vector from the potential function and  $\phi$  is the current bearing of the robot. When the commanded force resulting from steering proportioning exceeds the maximum tractive capability of the vehicle, slip control mode is triggered, and individual torque commands are scaled accordingly.

#### IV. CONTROL PERFORMANCE

The performance of the global potential function and local slip control in a cooperative path planning and control task is demonstrated here through simulation of a group of three robots moving on a low adhesion surface. As indicated in eq. 10-11, the robots interact with each other via the inter-vehicle potential, and the degree of interaction is adjusted by scalar gain  $\alpha_d$ .  $d_o$  and  $h_o$  affect the way robots arrange themselves relative to each other and around the leader at steady-state. The inter-vehicle potential also reduces the potential for collision. The task is for robots to arrange themselves on a circle around a virtual leader or target, starting from a distance of roughly 100 m from the target. The potential function parameters are tuned for the high adhesion terrain; hence, the simulation is a test of robustness of the cooperative control framework to adhesion conditions.

Figure 7 shows the trajectories of each robot during global formation control on a low adhesion surface, with and without slip control active. The vehicles start parallel to each other, thus the two flanking vehicles start with a bearing error and must execute a turn, with net force applied to the vehicle being a result of both the potential function force, and the steering control law. The circle represents the well of the virtual leader's potential function, or the "stopping point" for the robots. The simulation time is 35 sec. for each slip control condition. With slip control inactive, the commanded forces from the potential function cause the tire forces to saturate, resulting in high wheel slip and loss of traction during this high-velocity maneuver. The peak velocities of the flanking vehicles along the trajectory are 7.26 m/s, while the center vehicle's top speed is 7.29 m/s. The center vehicle overshoots its target by over 50 m. The flanking vehicles are unable to "repel" as per the interaction gain  $\alpha_d$ . These vehicles lose lateral stability just after they initiate the turn inwards ( $x$ -position of  $\sim 40$  m) and collide, as the force commands from the potential function are unable to be realized due to tire force saturation. With slip control active, lateral stability is retained, and peak velocities are 6 m/s for flanking vehicles and 6.8 m/s for the center vehicle. Flanking robots "repel" starting early in the trajectory, and retain lateral adhesion as they move outward. The lack of symmetry in the trajectories under slip control is attributed to the interaction gain  $\alpha_d$  and its tendency to keep vehicles from colliding. The vehicles successfully reach the circle by 30 sec. While trajectories of the center and flanking vehicle overlap in Fig. 7, collision is avoided due to the difference in speed along individual robot trajectories.

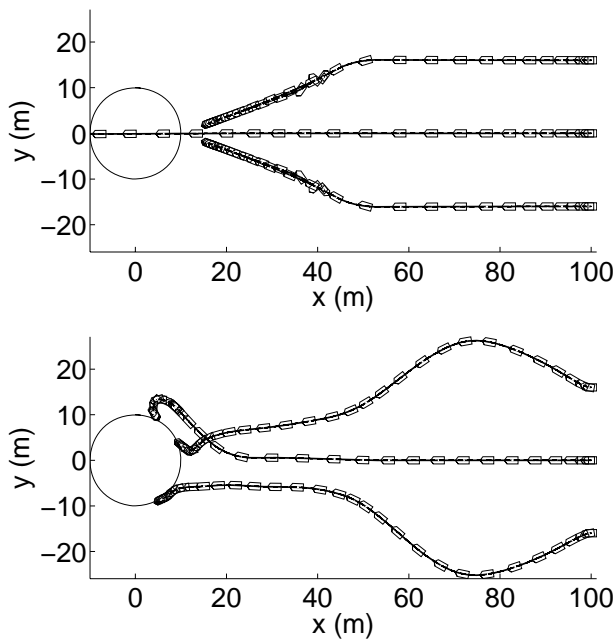


Figure 7 Group dynamics on a low adhesion surface. Top: slip control is inactive, bottom: slip control is active.

Future research will focus on experimental validation of the vehicle dynamic model, development and validation of tire-terrain interaction models, and experimental evaluation of the control framework with the robotic testbed.

#### V. CONCLUSIONS

Cooperative control strategies for high-speed emergency response depend significantly on terrain characteristics. Current cooperative control methods and terrain models do not adequately address dynamic behaviour of high-speed mobile robots. In response, this paper develops a baseline dynamic model of a high-speed mobile robot and presents a control framework for emergency response tasks requiring multiple robots operating at high speed. The framework, comprised of an existing global, dynamic path planning and motion controller and a local slip-based traction control, is shown to provide robust formation control on low adhesion terrain when the global controller is tuned for high adhesion terrain. A design and prototype for an inexpensive, lightweight, wheeled mobile robot serving as a testbed for studying high-speed cooperative control is summarized.

#### ACKNOWLEDGEMENTS

This research was supported by the National Institute of Standards under Grant No. 60NANB4D1144 and by the Institute for Security Technology Studies, through Grant No. 2005-DD-BX-1091 awarded by the Bureau of Justice Assistance.

#### REFERENCES

[1] 2004 Army Transformation Roadmap, United States Army, July 2004, [http://www.oft.osd.mil/library/library\\_files/document\\_386\\_ATR\\_2004\\_Final.pdf](http://www.oft.osd.mil/library/library_files/document_386_ATR_2004_Final.pdf).

- [2] H. Schempf, W. Crowley, C. Gasior, D. Moreau, Ultra-rugged Soldier-Robot for Urban Conflict Missions, Unmanned Systems 2003 Conference - AUVSI 30th Annual Symposium and Exhibition, Baltimore, MD, July 15-17, 2003.
- [3] Statement of Requirements for Urban Search and Rescue Robot Performance Standards, Dept. of Homeland Security Science and Technology Directorate and National Institute of Standards and Technology, May 2005, [http://www.isd.mel.nist.gov/US&R\\_Robot\\_Standards/Requirements%20Report%20\(prelim\).pdf](http://www.isd.mel.nist.gov/US&R_Robot_Standards/Requirements%20Report%20(prelim).pdf)
- [4] D. Calisi, A. Farinelli, L. Iocchi, D. Nardi, Autonomous Navigation and Exploration in a Rescue Environment, 2005 IEEE Int. Workshop on Safety Security, and Rescue Robotics, pp. 54-59, June 2005.
- [5] J.L. Du, S. Ruhup, U. Witkowski, U. Ruckert, *Resource and Service Discovery for Large-Scale Robot Networks in Disaster Scenarios*, IEEE Int. Workshop on Safety Security, and Rescue Robotics, pp. 7-12, June 2005.
- [6] B.J. Choi and S.V. Sreenivasan, Gross Motion Characteristics of Articulated Mobile Robots with Pure Rolling Capability on Smooth Uneven Surfaces, IEEE Trans. on Robotics and Automation, 15(2), 340-343, 1999.
- [7] A. Hamdy and E. Badreddin, Dynamic Modeling of a Wheeled Mobile Robot for Identification, Navigation and Control", IMACS Conf. on Modeling and Control of Technological Systems, 119-128, 1992.
- [8] S. Shekhar, Wheel Rolling Constraints and Slip in Mobile Robots, Proc. of the IEEE Int. Conf. on Robotics and Automation, 3, 2601-2607, 1997.
- [9] R. L. Williams II and B. E. Carter, P. Gallina, and G. Rosati, Dynamic Model with Slip for Wheeled Omni-Directional Robots, IEEE Trans. on Robotics and Automation 18(3), 285-293, 2002.
- [10] K. Iagnemma, A Laboratory Single-Wheel Testbed for Studying Planetary Rover Wheel-Terrain Interaction, Technical Report 01-05-05, MIT Field and Space Robotics Laboratory.
- [11] H. Pacejka and E. Bakker, The Magic Formula Tyre Model, Proc. 1<sup>st</sup> International Colloquium on Tyre Models for Vehicle Dynamics Analysis, 1-18, 1991.
- [12] O. Khatib, Real time obstacle avoidance for manipulators and mobile robots, Int. J. Robotics Res., 4(4), 32-46, 1986.
- [13] W.S. Newman and N. Hogan, High speed robot control and obstacle avoidance using dynamic potential functions, Proc. IEEE. Int. Conf. Robotics and Automation, 14-24, 1987.
- [14] E. Rimon and D. Koditschek, Exact robot navigation using artificial potential functions, IEEE Trans. On Robotics and Automation, 8(5), 501-518, Oct 1992.
- [15] P. Ögren, E. Fiorelli and N. Leonard, Cooperative Control of Mobile Sensor Networks: Adaptive Gradient Climbing in a Distributed Environment, IEEE Trans. on Automatic Control, 49(8), 1292-1302, Aug. 2004.
- [16] L.R. Ray, Nonlinear Tire Force Estimation and Road Friction Identification: Simulation and Experiments. *Automatica*, 33(10), pp. 1819-1833, 1997.